

Ecological and hydroclimatic determinants of vegetation water-use strategies

Received: 11 October 2024

Accepted: 24 June 2025

Published online: 29 July 2025

 Check for updates

Bryn E. Morgan^{1,2,5}✉, Ryoko Araki^{1,3}, Anna T. Trugman^{1,2} & Kelly K. Caylor^{1,2,4}

Vegetation responses to soil moisture limitation play a key role in land–atmosphere interactions and are a major source of uncertainty in future projections of the global water and carbon cycles. Vegetation water-use strategies—that is, how plants regulate transpiration rates as the soil dries—are highly dynamic across space and time, presenting a major challenge to inferring ecosystem responses to water limitation. Here we show that, when aggregated globally, water-use strategies derived from point-based soil moisture observations exhibit emergent patterns across and within climates and vegetation types along a spectrum of aggressive to conservative responses to water limitation. Water use becomes more conservative, declining more rapidly as the soil dries, as mean annual precipitation increases and as woody cover increases from grasslands to savannahs to forests. We embed this empirical synthesis within an ecohydrological framework to show that key ecological (leaf area) and hydroclimatic (aridity) factors driving demand for water explain up to 77% of the variance in water-use strategies within ecosystem types. All biomes respond to ecological and hydroclimatic demand by shifting towards more aggressive water-use strategies. However, woodlands reach a threshold beyond which water use becomes increasingly conservative, probably reflecting the greater hydraulic risk and cost of tissue damage associated with sustaining high transpiration rates under water limitation for trees than grasses. These findings highlight the importance of characterizing the dynamic nature of vegetation water-use strategies to improve predictions of ecosystem responses to climate change.

Plant transpiration accounts for 60–80% of water fluxes from the land surface to the atmosphere^{1,2} and plays a major role in the global water cycle. Because plants are often under water stress³, water-limited transpiration, where plants downregulate stomatal conductance in response to decreased water availability, constitutes an important and substantial component of the global water budget. Plant water use is inherently linked to productivity and temperature through photosynthesis, so plant responses to water limitation mediate not just water fluxes but carbon⁴ and energy fluxes⁵ as well. Despite its importance,

however, the sensitivity of vegetation to water stress remains a major source of uncertainty in future projections of the water and carbon budgets^{6,7}. Reducing this uncertainty requires understanding how plants adjust to changing hydroclimatic and environmental conditions and the impact of these responses on overall ecosystem productivity and water use⁸.

The effect of water limitation, typically characterized by soil moisture stress, on plant transpiration and productivity is widely variable across different plant functional types and climate conditions^{9–11}.

¹Department of Geography, University of California, Santa Barbara, Santa Barbara, CA, USA. ²Earth Research Institute, University of California, Santa Barbara, Santa Barbara, CA, USA. ³Department of Geography, San Diego State University, San Diego, CA, USA. ⁴Bren School of Environmental Science and Management, University of California, Santa Barbara, Santa Barbara, CA, USA. ⁵Present address: Department of Civil and Environmental Engineering, Massachusetts Institute of Technology, Cambridge, MA, USA. ✉e-mail: brynmorgan@ucsb.edu

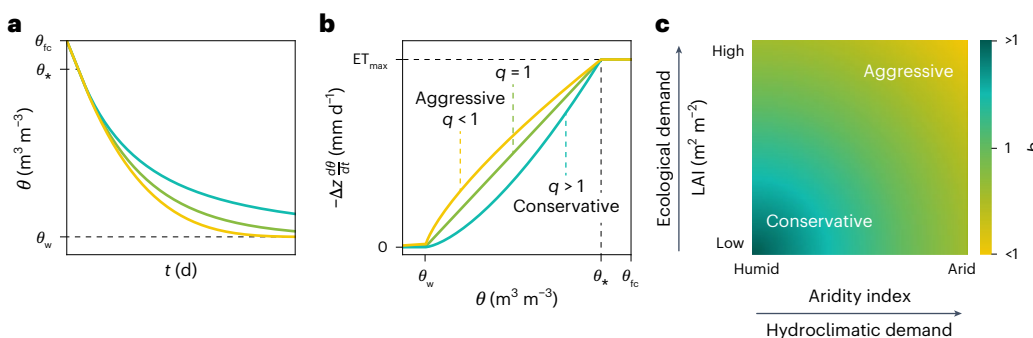


Fig. 1 | Emergent patterns of vegetation water use from soil moisture dynamics. **a**, The decline in volumetric soil water content θ over a drydown event. **b**, The soil moisture loss function, $-\Delta z \frac{d\theta}{dt}$ (mm d⁻¹), equivalent to ET when $\theta_w < \theta \leq \theta$. Between the field capacity, θ_{fc} , and the critical point, θ_* , ET occurs at a maximum rate, ET_{max} . Below θ_* , the green lines in **a** and **b** correspond to the linear model in

which $q = 1$. The yellow lines represent an aggressive water-use strategy ($q < 1$) and the blue lines represent a conservative strategy ($q > 1$). **c**, The hypothesized sensitivity of q to ecological and hydroclimatic demand. Under humid conditions and low LAI, plants are expected to use water conservatively. Increased demand causes a shift towards more aggressive water use, reflected by a decrease in q .

Some plants downregulate carbon uptake and water use in response to declining water availability to avoid mortality; others maximize carbon uptake until available moisture is exhausted¹². Maintaining high transpiration rates in spite of water limitation can be considered a more ‘aggressive’ water-use strategy due to the increasing risk of hydraulic damage and results in faster depletion of available soil moisture following rainfall events. Conversely, a more ‘conservative’ strategy involves downregulating transpiration when water is limited to maintain plant water status and preserves soil moisture for a longer period of time¹³. These responses to water stress are inherently related to ecosystem-scale fluxes¹⁴ and are associated with drought resilience^{15,16}, so characterization of vegetation water-use strategies can provide critical insight into ecosystem function.

A major challenge to characterizing vegetation water-use strategies is that they can vary over space and time in response to changes in ecological and hydroclimatic drivers¹⁷. In general, when water is abundant relative to ecological demand (that is, leaf area index, LAI (m² m⁻²)) or hydroclimatic demand (that is, potential evapotranspiration, PET), water use is more conservative¹⁸, and moisture is retained in the soil for longer (Fig. 1). However, when that water may be used by neighbouring plants, higher transpiration rates provide a competitive advantage to prevent water losses to neighbours^{19,20}. Thus, as LAI increases for a given vegetation type, water-use strategies should become more aggressive. Alternatively, increased atmospheric demand can induce more aggressive water use, both via excess water loss through the stomata and via soil evaporation²¹. Atmospheric or hydroclimatic demand is driven by the balance between rainfall and PET, defined as the aridity index (AI (–)). As aridity increases, water-use strategies should become more aggressive due to the stronger moisture gradient from the soil through the plant to the atmosphere (Fig. 1c). Importantly, the ability of plants to adjust to changing conditions can affect ecosystem resilience to and recovery from drought stress¹⁶, but predicting plant responses to water limitation based on vegetation type²² or climate²³ alone is challenging. Thus, quantifying the extent to which vegetation water-use strategies in different ecosystems shift in response to temporally varying factors including ecological and hydroclimatic demand is crucial for understanding ecosystem responses to water stress.

Soil moisture (θ (m³ m⁻³)) is a key variable that links fluxes of water between the land surface, vegetation and the atmosphere²⁴. Parameters describing plant water uptake can be derived from the time evolution of soil moisture following rainfall^{24,25}, when water is lost from the soil to various sources (that is, drydown events). In the latter stages of soil drydowns, plant water uptake or transpiration (ET (mm d⁻¹)) dominates the loss function, so the change in θ over

time, $\frac{d\theta}{dt}$ (m³ m⁻³ d⁻¹), can be attributed to vegetation water use and is given by the equation^{25–27}:

$$-\Delta z \frac{d\theta}{dt} = ET(\theta, t) = ET_{max} \left(\frac{\theta(t) - \theta_w}{\theta_* - \theta_w} \right)^q, \quad (1)$$

where Δz is the depth of the soil layer (m), $\theta(t)$ is the volumetric soil moisture (m³ m⁻³) at time t (d), ET_{max} (mm d⁻¹) is the maximum transpiration rate, θ_w (m³ m⁻³) is the wilting point when transpiration stops, θ_* (m³ m⁻³) is the point of incipient stomatal closure²⁵ and q (–) is a new parameter introduced here that describes the nonlinearity of vegetation responses to declining water availability (Fig. 1). Critically, in prior estimations q has been implicitly assumed to be 1, representing a linear plant response to soil drying.

Here we characterize vegetation water-use strategies across biomes using a nonlinear parameterization of equation (1) to describe the ET– θ relationship in the water-limited drydown stage ($q \neq 1$). In addition to characterizing patterns of water-use strategies by vegetation type and climate, we focus on the dynamic response of q to ecological and hydroclimatic drivers. We use the nonlinear parameter q to quantify the degree to which water-use strategies are more aggressive ($q < 1$)—where water use is sustained as the soil dries—or conservative ($q > 1$)—where water use rapidly declines as the soil dries—under water limitation (Fig. 1b). Representing plant sensitivity to increasing water scarcity, q is thus a useful metric for diagnosing differences in vegetation water-use strategies as the soil dries down.

We address the following three questions: (1) what are the global patterns of water-use strategies—as measured by q —across vegetation types and climates? (2) How do these water-use strategies shift as demand for water increases? And (3) do different vegetation types respond in distinct ways to increasing ecological and hydroclimatic demand? To do so, we use soil moisture data from the International Soil Moisture Network (ISMN), a network of in situ soil moisture measurements at 3,095 sites across the globe (Fig. 2). We compare q values for all drydown events by vegetation type (grassland, savannah, woodland/forest) and climate (mean annual precipitation, MAP (mm)). We then evaluate how vegetation water-use strategies vary with increasing ecological (leaf area index, LAI (m² m⁻²)) and hydroclimatic (antecedent aridity index, AI₆₀ (–)) demand for water.

Results and discussion

Water-use strategies vary systematically by vegetation type and climate

The nonlinear parameter, q , introduced here captures differences in water-use strategies that follow coherent patterns across ecosystem

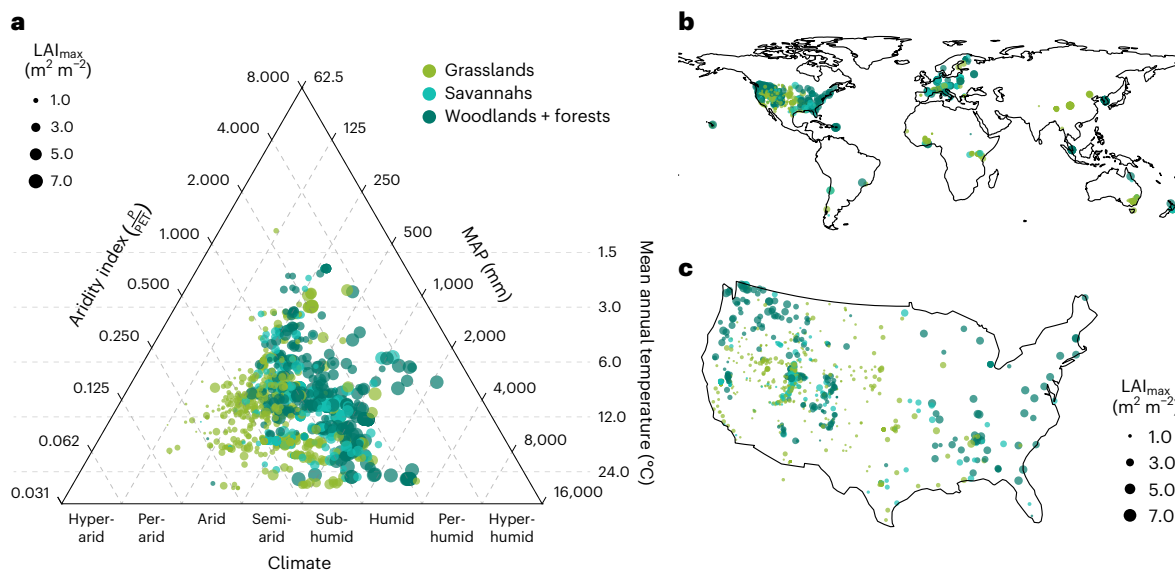


Fig. 2 | Biogeographic and geographic distributions of ISMN stations. **a–c**, Biogeography of the ISMN stations (**a**) included in the analysis and their distribution across the globe (**b**) and in the USA (**c**). A total of 26,747 drydown events from 1,268 stations were included in the analysis. Each of the stations used

is represented by a point. The size of each point represents the average maximum annual LAI, LAI_{\max} . For stations whose land-cover type changed over the study period, the woodiest category was used. Data in **a** from ref. 70.

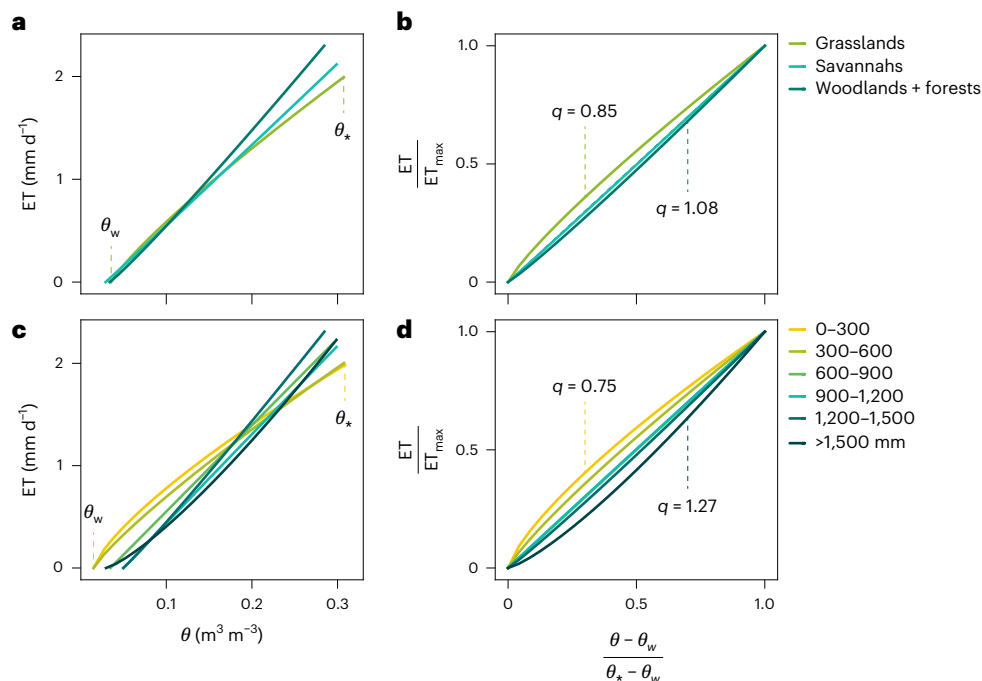


Fig. 3 | Median soil moisture loss functions by vegetation type and rainfall. **a–d**, The soil moisture loss functions in the water-limited evapotranspiration stage ($\theta_w \leq \theta \leq \theta_*$) are plotted by vegetation type (**a,b**) and mean annual rainfall (**c,d**). Median fitted parameters (θ_w , θ_* , ET_{\max} , and q) for each category were used to plot the curves in **a** and **c** according to equation (1). Normalized curves are shown in **b** and **d** annotated with median q values for endmember categories. Grasslands had the lowest median q values (0.85 , 95% CI [0.83 , 0.87], $n = 11,252$),

followed by savannahs (1.01 , 95% CI [0.97 , 1.05], $n = 5,909$) and woodlands (1.08 , 95% CI [1.05 , 1.1], $n = 9,586$), which had the highest q values (Extended Data Table 1). Distributions of q values by vegetation type and rainfall bin are shown in Extended Data Fig. 1. Uncertainty estimates for the medians were determined via bootstrapping (Methods); the distributions of resampled medians are shown in Extended Data Fig. 2.

and climate types. Lower q values (median \pm standard error) were found in grasslands (0.85 ± 0.015) and arid regions (Fig. 3 and Extended Data Figs. 1 and 2), indicating that these places are characterized by vegetation with more aggressive water-use strategies, with sustained high transpiration rates as the soil dries. These findings can be explained by the physiology and hydraulic traits of vegetation in these places. Low q

values reflect the intrinsic nature of water use in grasslands, whereby grasses respond quickly to rainfall events, transpire more under stress and senesce when moisture is exhausted²⁴. Woody vegetation, on the other hand, tends to be less resistant to cavitation than herbaceous species²⁸ and is more sensitive to declining soil moisture²⁹, reflected here by higher median q values in woodland and forest ecosystems

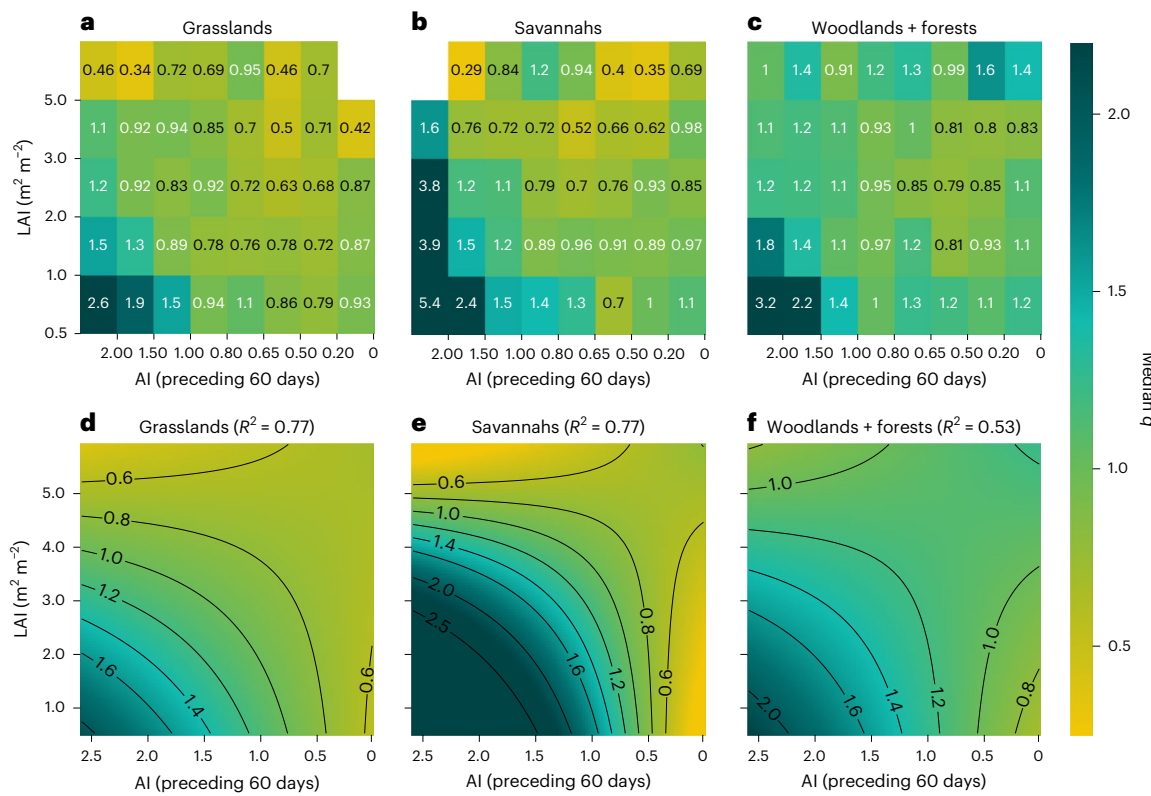


Fig. 4 | Median q values as a function of antecedent aridity and LAI by vegetation type. Antecedent aridity, AI_{60} , is calculated as the ratio of the total precipitation to the total PET in the 60 days preceding a drydown event; thus, aridity increases with decreasing AI_{60} . **a–c**, Observed median q values for grasslands (**a**), savannahs (**b**) and woodlands (**c**). Bins were chosen using aridity classifications⁷¹ (arid, $\text{AI} < 0.2$; semi-arid, $0.2 < \text{AI} < 0.5$; dry subhumid, $0.5 < \text{AI} < 0.65$) and based on the spread of humid events ($\text{AI} > 0.65$). LAI bins were

designated based on the spread of events. We use a threshold of $\text{LAI} > 0.5$ to eliminate events when bare soil evaporation probably dominates the drydown signal. **d–f**, Predicted median q values for grasslands (**d**), savannahs (**e**) and woodlands (**f**). Surfaces were fit using least squares regression to an equation of the form $q(\text{AI}_{60}, \text{LAI}) = c_{\text{AI}_{60}} \text{AI}_{60} + c_{\text{LAI}} \text{LAI} + c_{\text{AI}_{60}, \text{LAI}} \text{AI}_{60} \text{LAI} + c$. Coefficients $c_{\text{AI}_{60}}$, c_{LAI} , $c_{\text{AI}_{60}, \text{LAI}}$ and c are given in Extended Data Table 2.

(1.08 ± 0.017 ; Extended Data Table 1). These trends are also consistent with remote sensing studies showing that grasslands can extract water from drier soils³⁰ and are more anisohydric³¹ than woodier vegetation types. Water-use strategies in savannahs reflect their mixed tree–grass composition, with q values between grassland and woodland ecosystems (1.01 ± 0.029). In addition, we find more aggressive water use (lower q values) in arid regions, which is consistent with the anisohydric behaviour of dryland plants³² and their more drought-resistant water uptake strategies compared to mesic species^{33,34}. Cavitation resistance also increases with decreasing annual rainfall for both woody³⁵ and non-woody vegetation³⁶, allowing dryland vegetation to withstand higher levels of water stress, which further explains the increase in q values with MAP. These differences in q by vegetation and climate type highlight the importance of accounting for the nonlinearity of soil moisture drydowns to accurately capture ecohydrological dynamics across different ecosystems.

These coherent patterns of water use emerge despite the well-documented heterogeneity of soil moisture³⁷, highlighting the efficacy of aggregating dynamical metrics such as q derived from point-based soil moisture observations for understanding global patterns of vegetation water-use strategies. Previous advancements in understanding plant functional dynamics and water-use strategies from hydrological data have largely relied on landscape-scale observations from satellites^{22,30,31} or flux towers^{38,39}. A common theme of these studies is that vegetation type is not a strong predictor of responses to water stress, quantified by metrics such as the degree of isohydricity²² or critical soil moisture thresholds, θ_c ⁴⁰. The weak relationship between ecosystem type and these metrics can be explained

by the heterogeneity of plant responses, the availability of relevant datasets and the applicability of the metrics themselves. First, both soil moisture³⁷ and plant responses^{41,42} vary at much finer scales than that of multiple-km-resolution satellite pixels. Thus, differences in plant dynamics and responses to water limitation may be obfuscated at the ecosystem scale⁴³, where climate and large-scale hydrological processes dominate over vegetation-specific dynamics⁴⁴. Moreover, satellite-based soil moisture data are not available in forested areas⁴⁵, so they cannot be used to reveal differences based on woody cover, such as between trees and grasses. Meanwhile, ecosystem-scale flux data from towers are available at far fewer than the nearly 3,000 sites for which in situ soil moisture data are available. As a result, in this study, by retrieving the signatures of vegetation water use from point-based soil moisture dynamics alone, our analysis includes a broader range of vegetation types from a larger, more representative sample of ecosystems. Finally, compared with threshold-based metrics such as θ_c , q is less dependent on soil texture (Extended Data Fig. 3) and is thus a more robust metric for quantifying vegetation responses to water limitation. Thus, here we leverage fine-resolution soil moisture observations to reveal coherent patterns of water use by aggregating a novel, nonlinear parameter q , by vegetation type and climate rather than relying on aggregated observations of soil moisture values themselves or direct observations of plant water use. This approach capitalizes on the integrative nature of soil moisture, which reflects the dynamics of water fluxes between the land surface, vegetation and the atmosphere, to derive an interpretable metric for plant behaviour that can be difficult to detect from ecophysiological data. Our findings suggest that water-use strategies are, in fact, strongly related to

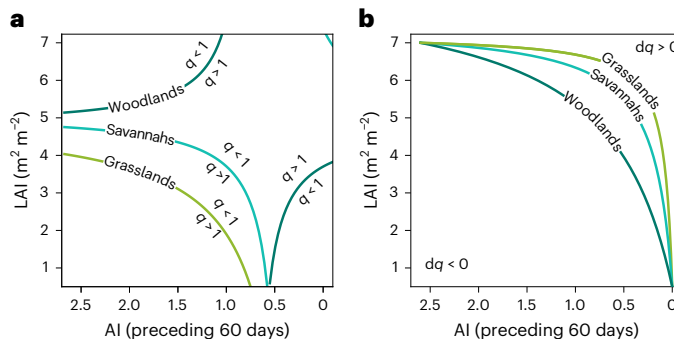


Fig. 5 | Patterns of q by vegetation type. **a**, Isolines at $q = 1$ by vegetation type. Values of q below 1 indicate more aggressive water use. **b**, Minimum q ('maximum aggression') as a function of antecedent aridity and LAI. The curves in **b** represent where water use is most aggressive (that is, q is minimized) for each vegetation type. Below this line, q decreases with increasing LAI and aridity ($dq < 0$); above this line, q increases ($dq > 0$). In the case of grasslands, which seldom reach LAI much higher than $\sim 5 \text{ m}^2 \text{ m}^{-2}$, this threshold is unlikely to be reached; rather, q continues to decline as demand increases for all realistic LAI values. Methods provide a detailed explanation of how these curves are derived.

ecosystem type, despite the difficulty of detecting these differences using other metrics derived from ecosystem-scale observations.

Water-use strategies respond dynamically to demand within vegetation types

Beyond analysing the overall biogeographic patterns of water use, we also introduce a framework that reveals dynamical plant responses to ecological and hydroclimatic demand for water, highlighting the plasticity of plant responses to water limitation. Together, LAI and antecedent aridity—defined as the aridity index of the 60 days preceding the start of a drydown event—explain 76.6% of the variance in median q values of both grasslands and savannahs and 52.6% of the variance in median q values of woodlands (Fig. 4 and Extended Data Table 2). In grasslands and savannahs, increasing demand for water from both biotic and abiotic sources leads to more aggressive water use (lower q values). In woodlands, however, water-use strategies showed similar trends of decreasing q values, but only up to intermediate LAI and AI values. As LAI and aridity continue to increase, water-use strategies in woodlands become more conservative (higher q values) when demand is very high (Fig. 4); that is, woodlands reach a threshold of ecological and hydroclimatic demand beyond which increasingly aggressive water use is no longer sustainable. As a result, while grasslands and savannahs exhibit the most aggressive water use (lowest q values) at maximum LAI and minimum AI_{60} , water use in woodlands is most aggressive (that is, q is minimized) when LAI and aridity are lower (Fig. 5).

These differences in responses to ecological and hydroclimatic demand between ecosystem types reflect the risk–benefit trade-offs of changing water-use strategies. The benefit of a more aggressive water-use strategy (decreasing q) is an increase in overall water use, but this comes with greater hydraulic risks. Sustaining high transpiration rates when water is limited leads to decreased plant water potentials, embolism and, ultimately, mortality^{46,47}. Woody vegetation tends to be more vulnerable to hydraulic failure than herbaceous vegetation²⁸, so trees are more sensitive to declining soil moisture than grasses^{29,48}. Moreover, whereas grasses can senesce when soil moisture is depleted⁴⁹, the carbon costs of potentially catastrophic hydraulic failure are much greater for trees, which have more structural aboveground biomass that must survive over many years²⁰. As a result, water-use strategies transition from more conservative ($q > 1$) to more aggressive ($q < 1$) at lower LAI and higher AI_{60} values in grasslands than woodlands and forests (Fig. 5). Given the importance of leaves in the hydraulic pathway⁵⁰ and their vulnerability to water stress⁵¹, higher LAI

could increase the risk of tree embolism when compounded with arid conditions, during which water stress can be higher due to elevated atmospheric demand⁵². Thus, the return towards more conservative water use in woodlands and forests when LAI is high and conditions are dry probably reflects the different traits and life history strategies of trees relative to grasses, which transpire most aggressively when competition is highest (Figs. 4 and 5).

This Article shows that ecological and hydroclimatic factors are key determinants of plant water-use strategies across herbaceous and woody vegetation types. Previous work using other response-based metrics has highlighted the difficulty of surfacing global patterns²² and scaling site-specific insights²³. Utilizing a global database of surface soil moisture, we derive vegetation-specific distributions of the nonlinearity in plant water use response to soil moisture drydowns, q , which we show to vary consistently within and between vegetation types. We embed our empirical synthesis within an ecohydrological framework, and we use this framework to characterize the dynamical nature of plant water-use strategies in response to key biotic (LAI) and hydroclimatic (AI_{60}) factors that drive demand for limited water resources. This integration of ecohydrological theory and empirical synthesis suggests that q —and its relationship to LAI and AI_{60} —is a valuable tool for assessing dynamical vegetation responses to water limitation and, in turn, improving understanding of how plant water-use strategies affect global water and carbon fluxes.

Methods

Theory

Following a rainfall event, water is lost from a volume of soil through surface runoff, leakage into deeper subsurface layers and evapotranspiration, $ET(\theta, t)$ (mm d^{-1}) in three phases^{25,26}. In the initial drainage stage, the soil moisture loss function, $\frac{d\theta}{dt}$, is dominated by runoff and leakage, which occur rapidly until θ reaches field capacity⁵³. The subsequent stages are dominated by evapotranspiration (Fig. 1), which occurs at a maximum rate (ET_{\max}) until some critical threshold θ_c is reached, at which point plants begin closing their stomata to prevent excess water loss^{54–56}. That is

$$-\Delta z \frac{d\theta}{dt} = ET(\theta, t) = \begin{cases} ET_{\max} & \theta_c < \theta \leq \theta_f \\ ET_{\max} \left(\frac{\theta(t) - \theta_w}{\theta_f - \theta_w} \right) & \theta_w < \theta \leq \theta_c \end{cases} \quad (2)$$

where Δz is the depth of the soil layer (m), $\theta(t)$ is the volumetric soil moisture ($\text{m}^3 \text{ m}^{-3}$) at time t (d), θ_f is the field capacity of the soil ($\text{m}^3 \text{ m}^{-3}$) and θ_w ($\text{m}^3 \text{ m}^{-3}$) is the wilting point, the value of soil moisture at which transpiration stops²⁵. Consistent with previous definitions^{25,26}, θ_w is conceptualized here as the value of soil moisture at which the matric potential is too low for water to be extracted by plants. The critical point, θ_c , represents the threshold of soil moisture beyond which vegetation water use becomes water limited^{54–56}.

Equation (2) implies a linear relationship between ET, dominated by transpiration, and θ in the water-limited stage ($\theta_w < \theta \leq \theta_c$; Fig. 1). We modify this portion of equation (2) to introduce a nonlinear parameter, q , which describes the shape of the loss function as a function of θ (equation (1))⁵⁷. In equation (1), when $q = 1$, the loss function is linear. Critically, q enables for the representation of diverse observed water-use strategies that diverge depending on vegetation type. For example, when $q > 1$, the loss function is concave up, indicating more conservative water uptake with plants shutting down transpiration more rapidly as the soil dries down. On the other hand, $q < 1$ indicates a more aggressive water-use strategy in which transpiration continues until nearly all available soil moisture is exhausted (Fig. 1b).

Data

We use in situ soil moisture data from the International Soil Moisture Network (ISMN)^{58,59} to derive q and characterize drydown regimes.

The ISMN contains data from 80 regional networks and 3,095 stations across the globe, which have been compiled into a standardized format and flagged for quality issues. Soil moisture data are available from 11,676 sensors at different depths and for different time periods.

Data for each sensor were filtered for good-quality data using ISMN quality flags and averaged to daily values. The depth of each sensor was taken as the lower bound of the reported soil layer depth in the ISMN metadata. This ensured consistency across all sensors, as many report only a single depth. We included measurements up to 50-cm deep to cover the majority of the plant root zone^{60,61} without large differences in Δz substantially impacting the results.

For each sensor, soil texture information was extracted using the GLDAS dataset⁶², which includes data for the surface layer (0–0.3 m) and a deeper soil layer (0.3–1.0 m). Soil texture was used to determine field capacity, θ_{fc} , for the location and depth of the sensor using the water retention curves of Clapp and Hornberger (1978)⁶³.

We compared values of q by vegetation type, aridity and leaf area index (LAI ($m^2 m^{-2}$)). Vegetation functional types were derived from the International Geosphere-Biosphere Programme (IGBP) classification using the MODIS Terra+Aqua Combined Land Cover product (MCD12Q1), version 6.1⁶⁴, which provides yearly land-cover data from 2001 through 2022. We focused on three broad categories: grasslands, savannahs and woodlands/forests. Grasslands and savannahs were defined according to the IGBP definitions, and we combined woodier vegetation types (that is, woody savannahs and all forest types) into a single class to focus on differences between trees and grasses. Each drydown event was assigned to a vegetation class based on its location and date; whereas classification of most sites remained constant across the time period, land-cover changed at some sites, so events from one site may comprise multiple vegetation classes.

LAI was derived from the MODIS Terra+Aqua combined 8-day composite product (MCD15A2H)⁶⁵, which provides global LAI estimates at 500-m resolution. LAI data were filtered for bad data based on the quality flags and forward-filled within each 8-day period of the temporal composite. The maximum LAI value for each drydown event was used as measure of ecological demand to ensure consistency and robustness across events, which may span one or more 8-day periods.

To evaluate climatic factors, we calculated the mean annual precipitation (MAP (mm)) for each site, and the aridity index (AI (–)), which is the ratio of precipitation to potential evapotranspiration (PET). Precipitation data were derived from the Climate Hazards Group InfraRed Precipitation with Station data (CHIRPS), version 2.0 dataset⁶⁶ at 0.05° resolution. Daily PET values were extracted from the dPET dataset⁶⁷, which contains daily estimates of PET globally at 0.1° resolution. In addition to calculating mean AI for each site from the ratio of MAP to mean annual PET, we calculated the antecedent aridity index, AI_{60} , for the 60 days preceding the start of each drydown.

Implementation of drydown models

Identification of drydown events. Drydown events are episodes after rainfall in which a pulse of moisture is followed by declining soil moisture until the next rain event. For a given sensor, the start of a drydown event was identified as a period in which the decline in soil moisture was less than -0.5 mm d^{-1} for at least 6 consecutive days. The end of a drydown event was defined either by a decrease of less than -0.5 mm d^{-1} or an increase in θ ; that is, $\frac{d\theta}{dt} > -0.5 \text{ mm d}^{-1}$. The threshold of -0.5 mm d^{-1} represents the minimum allowed transpiration rate; soil moisture may continue to decline below this threshold to the hygroscopic point, though the suction is too high for plants to extract water and tissue damage occurs^{56,68}. The distributions of drydown event lengths are shown in Supplementary Fig. 2.

Model fitting. To derive model parameters, we fit the analytical solution of equation (1) to the observed θ values for each drydown event to

derive model parameters. This approach avoids compounded errors in the calculated $\frac{d\theta}{dt}$ due to noise in the observed soil moisture data²⁷.

To compare the performance of the nonlinear model to the linear approach, we first fit the following exponential solution to equation (1) for the case when $q=1$ ^{27,69}:

$$\theta(t) = (\theta_0 - \theta_w) e^{-\frac{ET_{max}}{\Delta z(\theta_0 - \theta_w)} t} + \theta_w \quad (3)$$

where t is the time since the start of the drydown (d) and θ_0 is the initial soil moisture value $\text{m}^3 \text{ m}^{-3}$ at $t=t_0$.

For the case when $q \neq 1$, the analytical solution of equation (1) is:

$$\theta(t) = \left[-\frac{ET_{max}}{\Delta z} \frac{1-q}{(\theta_* - \theta_w)^q} t + (\theta_0 - \theta_w)^{1-q} \right]^{1/(1-q)} + \theta_w \quad (4)$$

In both equations (3) and (4), we use nonlinear least squares fitting to derive θ_* , θ_w , ET_{max} and q . In both equations, θ is constrained between θ_{fc} and θ_w . Because transpiration may not necessarily occur at the potential rate, ET_{max} is also derived from the model fit and is constrained between 0 and potential evapotranspiration (PET), derived from the dPET dataset. The maximum PET value during the drydown event was used as the upper bound on ET_{max} for the model fitting. The nonlinear parameter q was constrained to all positive numbers ($0 < q$). In equation (4), θ_w is taken to be the minimum soil moisture observed over the full time period; in equation (3), θ_w is a fitted parameter, bound between the minimum soil moisture value during the drydown event and the minimum observed value overall. In both cases, θ_w is an ‘effective’ wilting point that is probably smaller than the true value. However, given that the difference between the true point of zero transpiration and the hygroscopic point is very small, the effect of this difference on estimates of other parameters is probably minimal²⁷. The initial value, θ_0 , is the observed value at the start of the drydown. A comparison of goodness of fit between the linear and nonlinear models is shown in Supplementary Fig. 3.

For analysis, drydown events were filtered for goodness of fit ($R^2 > 0.7$), following McColl et al. (2017;²⁷) and spuriously low q values ($q > 0.01$). In addition, we only retained events for analysis in which total $d\theta$ over the course of the drydown—that is, plant-available water—was above a minimum threshold ($(\theta_0 - \theta_w) \geq 0.005 \text{ m}^3 \text{ m}^{-3}$ or 1 mm at $\Delta z = 0.2 \text{ m}$) and those with observed soil moisture values covering at least 20% of the total observed range across the time series.

Analysis. We compared parameter values by vegetation type and MAP. Differences in median values for the three vegetation types and rainfall ranges (0–300; 300–600; 600–900; 900–1,200; 1,200–1,500; >1,500 mm) were compared using non-parametric Kruskal-Wallis tests. Uncertainty estimates for median q values were determined using a bootstrapping procedure, which involved sampling q values for each group with replacement and calculating the median of the resampled values 1,000 times.

For each of the three vegetation types, we then examined the influence of ecohydrological demand on plant water use by deriving q as a function of LAI and antecedent aridity. We fit median q values and binned LAI and AI_{60} data to a multivariable linear equation of the form $q(AI_{60}, LAI) = c_{AI_{60}} AI_{60} + c_{LAI} LAI + c_{AI_{60}, LAI} AI_{60} LAI + c$, where c_x describes the relationship between variable x (AI_{60} or LAI) and q .

We use these coefficients and the isolines where $q=1$ to evaluate the effects of vegetation (LAI) and antecedent aridity (AI_{60}) on plant water-use strategies. In addition, we define a line of ‘maximum aggression’ where q approaches a local minimum with respect to either LAI or AI_{60} . This line represents the LAI value at which q is minimized for each value of AI_{60} (and vice versa). The derivation of this line is analogous to that of the steepest descent; because the global minima may be outside the bounds of realistic LAI and AI_{60} values (for example,

LAI greater than approximately 7 or $AI_{60} < 0$), we use a modified approach to approximate this line within the realistic physical bounds of each surface ($0.5 \leq LAI \leq 7 \text{ m}^2 \text{ m}^{-2}$; $0 \leq AI_{60} \leq 3$). We note that while maximum LAI values differ between ecosystem types, we use this global maximum to compare between categories. The line of maximum aggression is defined here as the trace of the response surface intersected by the plane containing the saddle point and the local minima at or near the maximum and minimum values of AI_{60} and LAI (that is, $(AI_{60,\max}, LAI_{\max}, q)$ and $(AI_{60,\min}, LAI_{\min}, q)$). The saddle point is defined as the point where the determinant $D(AI_{60}, LAI)$ is negative, where $D(x,y) = f_{xx}(x,y)f_{yy}(x,y) - (f_{xy}(x,y))^2$. The local minima are obtained numerically by searching for the lowest q values at the extrema of AI_{60} and LAI. In this case, the local minima were found at $(AI_{60,\max}, LAI_{\max}, q_i)$ and $(AI_{60,\min}, LAI_{\min}, q_j)$.

Reporting summary

Further information on research design is available in the Nature Portfolio Reporting Summary linked to this article.

Data availability

All soil moisture data used in this study are available from the International Soil Moisture Network^{58,59} (<https://ismn.earth/en/>). The PET data are available from ref. 67, accessible at <https://data.bris.ac.uk/data/dataset/qb8ujazzda0s2aykkv0oq0ctp>. CHIRPS rainfall data are available from the Climate Hazards Center (<https://www.chc.ucsb.edu/data/chirps>). MODIS Landcover and LAI data were retrieved from NASA's Application for Extracting and Exploring Analysis Ready Samples (AppEEARS; <https://appeears.earthdatacloud.nasa.gov>). GLDAS data are available at <https://ldas.gsfc.nasa.gov/gldas/soils>.

Code availability

All data processing and analyses were performed in Python 3.12. A custom Python package was developed to process the soil moisture drydowns and fit the nonlinear model. This package is available via GitHub at <https://github.com/ecohydro/drydowns>. The code for performing the analyses and creating the figures in this study is available via GitHub at <https://github.com/ecohydro/ismn-drydowns>.

References

- Jasechko, S. et al. Terrestrial water fluxes dominated by transpiration. *Nature* **496**, 347–350 (2013).
- Good, S. P., Noone, D. & Bowen, G. Hydrologic connectivity constrains partitioning of global terrestrial water fluxes. *Science* **349**, 175–177 (2015).
- Jiao, W. et al. Observed increasing water constraint on vegetation growth over the last three decades. *Nat. Commun.* **12**, 3777 (2021).
- Green, J. K. et al. Large influence of soil moisture on long-term terrestrial carbon uptake. *Nature* **565**, 476–479 (2019).
- Sellers, P. J. et al. Modeling the exchanges of energy, water, and carbon between continents and the atmosphere. *Science* **275**, 502–509 (1997).
- Trugman, A. T., Medvigy, D., Mankin, J. S. & Anderegg, W. R. L. Soil moisture stress as a major driver of carbon cycle uncertainty. *Geophys. Res. Lett.* **45**, 6495–6503 (2018).
- Swann, A. L. S., Hoffman, F. M., Koven, C. D. & Randerson, J. T. Plant responses to increasing CO_2 reduce estimates of climate impacts on drought severity. *Proc. Natl Acad. Sci. USA* **113**, 10019–10024 (2016).
- Zhang, B. et al. Species responses to changing precipitation depend on trait plasticity rather than trait means and intraspecific variation. *Funct. Ecol.* **34**, 2622–2633 (2020).
- Li, W. et al. Widespread and complex drought effects on vegetation physiology inferred from space. *Nat. Commun.* **14**, 4640 (2023).
- Wang, H. et al. Exploring complex water stress–gross primary production relationships: impact of climatic drivers, main effects, and interactive effects. *Glob. Change Biol.* **28**, 4110–4123 (2022).
- Feng, X. et al. The ecohydrological context of drought and classification of plant responses. *Ecol. Lett.* **21**, 1723–1736 (2018).
- Roman, D. T. et al. The role of isohydric and anisohydric species in determining ecosystem-scale response to severe drought. *Oecologia* **179**, 641–654 (2015).
- Rodríguez-Iturbe, I., Porporato, A., Laio, F. & Ridolfi, L. Intensive or extensive use of soil moisture: plant strategies to cope with stochastic water availability. *Geophys. Res. Lett.* **28**, 4495–4497 (2001).
- Anderegg, W. R. L. & Venturas, M. D. Plant hydraulics play a critical role in Earth system fluxes. *New Phytol.* **226**, 1535–1538 (2020).
- McDowell, N. et al. Mechanisms of plant survival and mortality during drought: why do some plants survive while others succumb to drought? *New Phytol.* **178**, 719–739 (2008).
- Anderegg, W. R. L. et al. Hydraulic diversity of forests regulates ecosystem resilience during drought. *Nature* **561**, 538–541 (2018).
- Feng, X. et al. Beyond isohydricity: the role of environmental variability in determining plant drought responses. *Plant Cell Environ.* **42**, 1104–1111 (2019).
- Lu, Y., Duursma, R. A. & Medlyn, B. E. Optimal stomatal behaviour under stochastic rainfall. *J. Theor. Biol.* **394**, 160–171 (2016).
- Zea-Cabrera, E., Iwasa, Y., Levin, S. & Rodríguez-Iturbe, I. Tragedy of the commons in plant water use. *Water Resour. Res.* <https://doi.org/10.1029/2005WR004514> (2006).
- Wolf, A., Anderegg, W. R. L. & Pacala, S. W. Optimal stomatal behavior with competition for water and risk of hydraulic impairment. *Proc. Natl Acad. Sci. USA* **113**, E7222–E7230 (2016).
- Massmann, A., Gentine, P. & Lin, C. When does vapor pressure deficit drive or reduce evapotranspiration? *J. Adv. Model. Earth Syst.* **11**, 3305–3320 (2019).
- Konings, A. G. & Gentine, P. Global variations in ecosystem-scale isohydricity. *Glob. Change Biol.* **23**, 891–905 (2017).
- Anderegg, L. D. L. Why can't we predict traits from the environment? *New Phytol.* **237**, 1998–2004 (2023).
- Rodríguez-Iturbe, I. & Porporato, A. *Ecohydrology of Water-Controlled Ecosystems* (Cambridge Univ. Press, 2005); <https://doi.org/10.1017/CBO9780511535727>
- Laio, F., Porporato, A., Ridolfi, L. & Rodríguez-Iturbe, I. Plants in water-controlled ecosystems: active role in hydrologic processes and response to water stress. II. *Adv. Water Resour.* **24**, 707–723 (2001).
- Rodríguez-Iturbe, I., Porporato, A., Ridolfi, L., Isham, V. & Cox, D. R. Probabilistic modelling of water balance at a point: the role of climate, soil and vegetation. *Proc. Math. Phys. Eng. Sci.* **455**, 3789–3805 (1999).
- McColl, K. A. et al. Global characterization of surface soil moisture drydowns. *Geophys. Res. Lett.* **44**, 3682–3690 (2017).
- Goedhart, C. M. & Pataki, D. E. Ecosystem effects of groundwater depth in Owens Valley, California. *Ecohydrology* **4**, 458–468 (2011).
- Kelliher, F. M., Leuning, R. & Schulze, E. D. Evaporation and canopy characteristics of coniferous forests and grasslands. *Oecologia* **95**, 153–163 (1993).
- Bassiouni, M., Good, S. P., Still, C. J. & Higgins, C. W. Plant water uptake thresholds inferred from satellite soil moisture. *Geophys. Res. Lett.* **47**, e2020GL087077 (2020).
- Li, Y. et al. Estimating global ecosystem isohydric/anisohydric using active and passive microwave satellite data. *J. Geophys. Res. Biogeosci.* **122**, 3306–3321 (2017).
- Garcia-Forner, N., Biel, C., Savé, R. & Martínez-Vilalta, J. Isohydric species are not necessarily more carbon limited than anisohydric species during drought. *Tree Physiol.* **37**, 441–455 (2017).

33. Vilagrosa, A. et al. in *Plant Responses to Drought Stress: From Morphological to Molecular Features* (ed. Aroca, R.) 63–109 (Springer, 2012); https://doi.org/10.1007/978-3-642-32653-0_3
34. Li, X. et al. Tree hydraulic traits are coordinated and strongly linked to climate-of-origin across a rainfall gradient. *Plant Cell Environ.* **41**, 646–660 (2018).
35. Choat, B. et al. Global convergence in the vulnerability of forests to drought. *Nature* **491**, 752–755 (2012).
36. Dória, L. C. et al. Embolism resistance in stems of herbaceous Brassicaceae and Asteraceae is linked to differences in woodiness and precipitation. *Ann. Bot.* **124**, 1–14 (2019).
37. Western, A. W. & Blöschl, G. On the spatial scaling of soil moisture. *J. Hydrol.* **217**, 203–224 (1999).
38. Xu, S. et al. Response of ecosystem productivity to high vapor pressure deficit and low soil moisture: lessons learned from the global eddy-covariance observations. *Earth's Future* **11**, e2022EF003252 (2023).
39. Fu, Z. et al. Critical soil moisture thresholds of plant water stress in terrestrial ecosystems. *Sci. Adv.* **8**, eabq7827 (2022).
40. Fu, Z. et al. Global critical soil moisture thresholds of plant water stress. *Nat. Commun.* **15**, 4826 (2024).
41. Anderegg, W. R. L. Spatial and temporal variation in plant hydraulic traits and their relevance for climate change impacts on vegetation. *New Phytol.* **205**, 1008–1014 (2015).
42. Lu, Y. et al. Intra-specific variability in plant hydraulic parameters inferred from model inversion of sap flux data. *J. Geophys. Res.: Biogeosci.* **127**, e2021JG006777 (2022).
43. Jarvis, P. G. & McNaughton, K. G. Stomatal control of transpiration: scaling up from leaf to region. *Adv. Ecol. Res.* **15**, 1–49 (1986).
44. Konings, A. G. et al. Tree species explain only half of explained spatial variability in plant water sensitivity. *Glob. Change Biol.* **30**, e17425 (2024).
45. Feldman, A. F., Akbar, R. & Entekhabi, D. Characterization of higher-order scattering from vegetation with SMAP measurements. *Remote Sens. Environ.* **219**, 324–338 (2018).
46. Tyree, T. & Sperry, J. S. Vulnerability of xylem to cavitation and embolism. *Annu. Rev. Plant Physiol. Mol. Biol.* **40**, 9–38 (1989).
47. McDowell, N. G. et al. Mechanisms of woody-plant mortality under rising drought, CO₂ and vapour pressure deficit. *Nat. Rev. Earth Environ.* **3**, 294–308 (2022).
48. Lu, Y., Duursma, R. A., Farrior, C. E., Medlyn, B. E. & Feng, X. Optimal stomatal drought response shaped by competition for water and hydraulic risk can explain plant trait covariation. *New Phytol.* **225**, 1206–1217 (2020).
49. Zavaleta, E. S. et al. Plants reverse warming effect on ecosystem water balance. *Proc. Natl Acad. Sci. USA* **100**, 9892–9893 (2003).
50. Sack, L., Cowan, P. D., Jaikumar, N. & Holbrook, N. M. The ‘hydrology’ of leaves: co-ordination of structure and function in temperate woody species. *Plant Cell Environ.* **26**, 1343–1356 (2003).
51. Brodribb, T. J., Holbrook, N. M., Edwards, E. J. & Gutiérrez, M. V. Relations between stomatal closure, leaf turgor and xylem vulnerability in eight tropical dry forest trees. *Plant Cell Environ.* **26**, 443–450 (2003).
52. Grossiord, C. et al. Plant responses to rising vapor pressure deficit. *New Phytol.* **226**, 1550–1566 (2020).
53. Rodriguez-Iturbe, I., D’Odorico, P., Porporato, A. & Ridolfi, L. On the spatial and temporal links between vegetation, climate, and soil moisture. *Water Resour. Res.* **35**, 3709–3722 (1999).
54. Hale, M. G. & Orcutt, D. M. *The Physiology of Plants Under Stress* (Wiley, 1987).
55. Larcher, W. *Physiological Plant Ecology: Ecophysiology and Stress Physiology of Functional Groups* (Springer, 1995).
56. Nilsen, E. T. & Orcutt, D. M. *Physiology of Plants Under Stress: Abiotic Factors* (Wiley, 1996).
57. Araki, R., Morgan, B. E., McMillan, H. K. & Caylor, K. K. Nonlinear soil moisture loss function reveals vegetation responses to water availability. *Geophys. Res. Lett.* **52**, e2024GL111403 (2025).
58. Dorigo, W. A. et al. The international soil moisture network: a data hosting facility for global in situ soil moisture measurements. *Hydrol. Earth Syst. Sci.* **15**, 1675–1698 (2011).
59. Dorigo, W. A. et al. The international soil moisture network: serving Earth system science for over a decade. *Hydrol. Earth Syst. Sci.* **25**, 5749–5804 (2021).
60. Feldman, A. F. et al. Remotely sensed soil moisture can capture dynamics relevant to plant water uptake. *Water Resour. Res.* **59**, e2022WR033814 (2023).
61. Dong, J., Lei, F. & Crow, W. T. Land transpiration-evaporation partitioning errors responsible for modeled summertime warm bias in the central United States. *Nat. Commun.* **13**, 336 (2022).
62. Rodell, M. et al. Basin scale estimates of evapotranspiration using GRACE and other observations. *Geophys. Res. Lett.* **31**, 10–13 (2004).
63. Clapp, R. B. & Hornberger, G. M. Empirical equations for some soil hydraulic properties. *Water Resour. Res.* **14**, 601–604 (1978).
64. Friedl, M. & Sulla-Menashe, D. MODIS/terra+aqua land cover type yearly L3 global 500m SIN grid V061. NASA Land Processes Distributed Active Archive Center <https://doi.org/10.5067/MODIS/MCD12Q1.061> (2022).
65. Myeni, R., Knyazikhin, Y. & Park, T. MODIS/terra+aqua leaf area index/FPAR 8-day L4 global 500m SIN grid V061. NASA Land Processes Distributed Active Archive Center <https://doi.org/10.5067/MODIS/MCD15A2H.061> (2021).
66. Funk, C. et al. The climate hazards infrared precipitation with stations—a new environmental record for monitoring extremes. *Sci. Data* **2**, 150066 (2015).
67. Singer, M. B. et al. Hourly potential evapotranspiration at 0.1° resolution for the global land surface from 1981–present. *Sci. Data* **8**, 224 (2021).
68. Lange, O. L., Kappen, L. & Schulze, E.-D. (eds) *Water and Plant Life: Problems and Modern Approaches* (Springer, 1976).
69. Rondinelli, W. J. et al. Different rates of soil drying after rainfall are observed by the SMOS satellite and the South Fork in situ soil moisture network. *J. Hydrometeorol.* **16**, 889–903 (2015).
70. Holdridge, L. R. *Life Zone Ecology* (Tropical Science Center, 1967).
71. UNEP *World Atlas of Desertification* (Edward Arnold, 1992).

Acknowledgements

B.E.M. and K.K.C. acknowledge support from the Zegar Family Foundation (grant number SB220237). B.E.M. acknowledges support from the Horton Research Grant from the American Geophysical Union. A.T.T. acknowledges funding from the National Science Foundation (grant number 2003205), the Gordon and Betty Moore Foundation (grant number GBMF11974), the USDI National Park Service (award numbers P24AC00910 and P24AC01425) and the CALFIRE Forest Health Research Program (grant number 60164685).

Author contributions

B.E.M. and K.K.C. designed the study. B.E.M. and R.A. wrote the code, and B.E.M. performed the analysis. B.E.M. wrote the paper with input from all co-authors. B.E.M., R.A., A.T.T. and K.K.C. provided input on the methodology and contributed to interpretation of the results.

Competing interests

The authors declare no competing interests.

Additional information

Extended data is available for this paper at <https://doi.org/10.1038/s41559-025-02810-8>.

Supplementary information The online version contains supplementary material available at <https://doi.org/10.1038/s41559-025-02810-8>.

Correspondence and requests for materials should be addressed to Bryn E. Morgan.

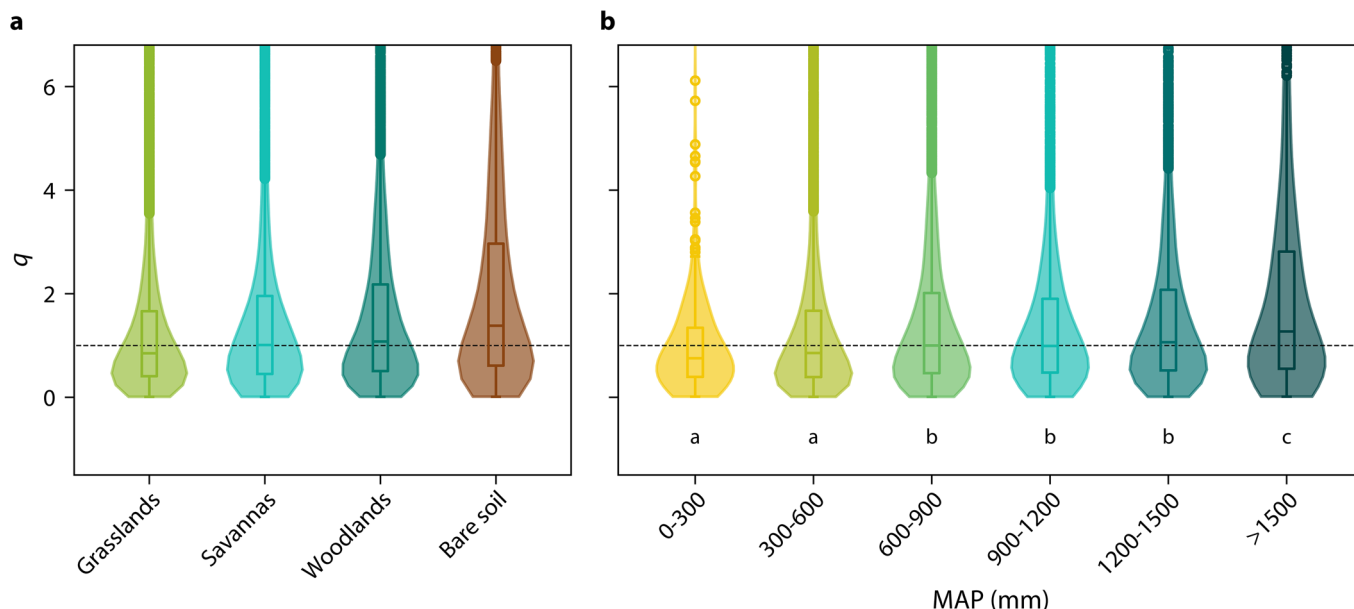
Peer review information *Nature Ecology & Evolution* thanks Maoya Bassiouni, Andrew F. Feldman and the other, anonymous, reviewer(s) for their contribution to the peer review of this work. Peer reviewer reports are available.

Reprints and permissions information is available at www.nature.com/reprints.

Publisher's note Springer Nature remains neutral with regard to jurisdictional claims in published maps and institutional affiliations.

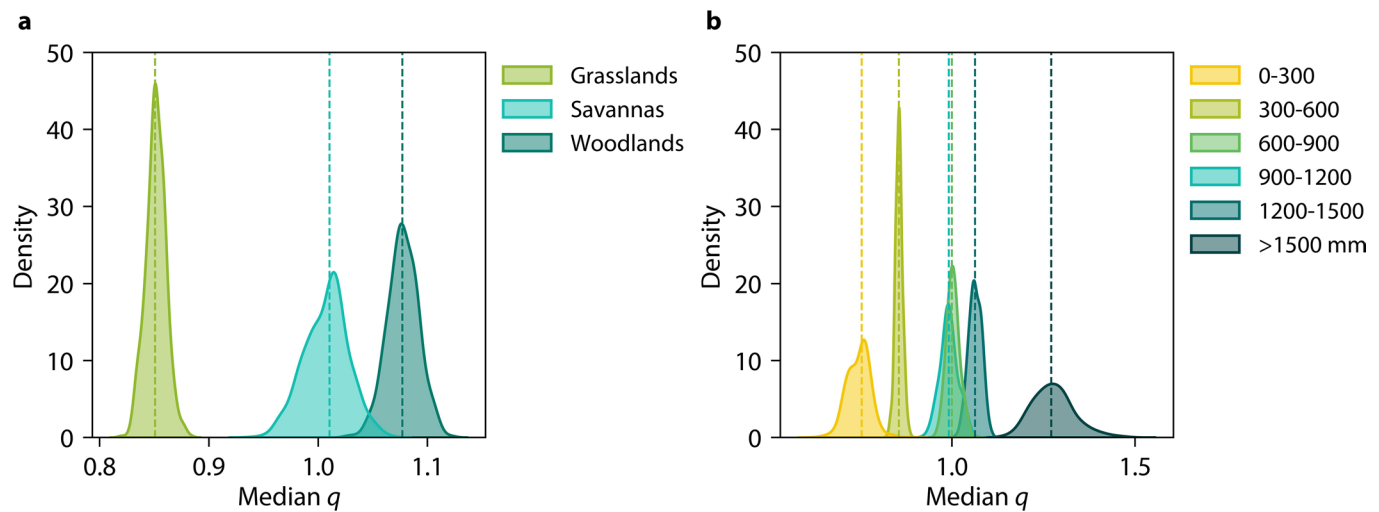
Springer Nature or its licensor (e.g. a society or other partner) holds exclusive rights to this article under a publishing agreement with the author(s) or other rightsholder(s); author self-archiving of the accepted manuscript version of this article is solely governed by the terms of such publishing agreement and applicable law.

© The Author(s), under exclusive licence to Springer Nature Limited 2025

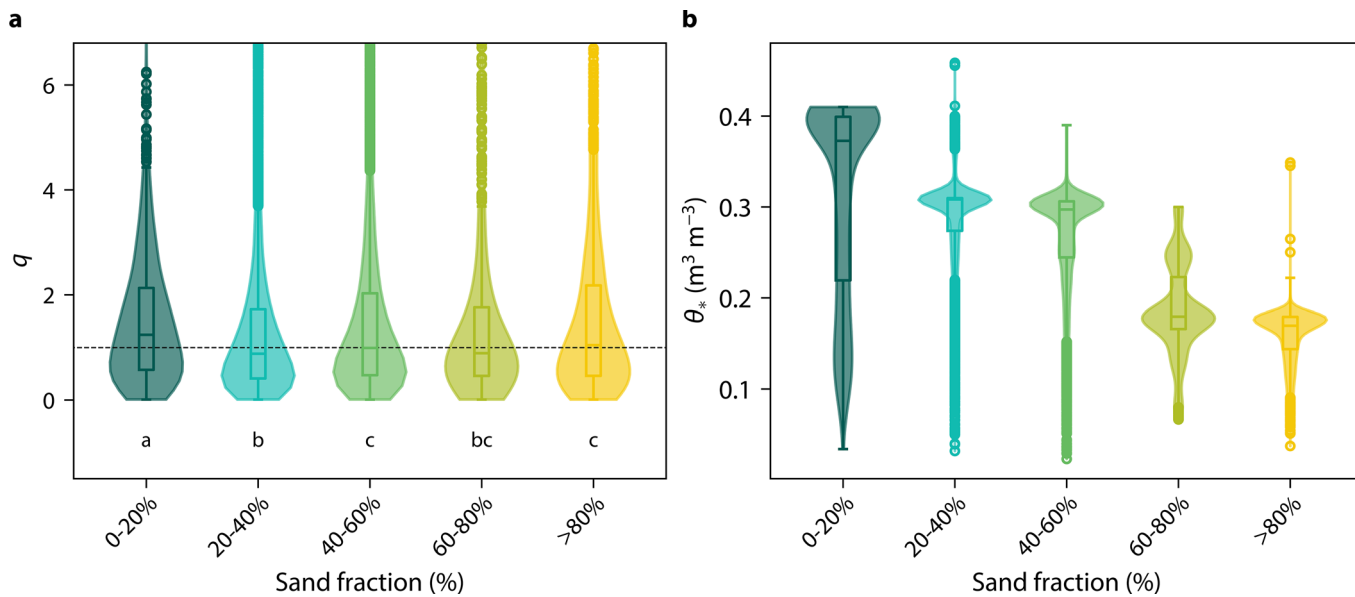


Extended Data Fig. 1 | Observed values of the nonlinear parameter, q , by (a) vegetation type and (b) mean annual precipitation. Violin plots show the distribution of q values in each category. Box plots show the medians and 25th to 75th percentile of q values; whiskers extend 1.5 times the inter-quartile range from each box. Outliers beyond this range are denoted by points. The dashed line shows where $q = 1$. Grasslands ($n = 11,252$), savannas ($n = 5,909$), woodlands ($n = 9,586$), and bare soil ($n = 3,507$) were significantly different from each other at $p < 0.001$ (two-sided Dunn's test with Bonferroni correction for multiple comparisons). Letters in (b) denote statistically significant differences between

median values ($p < 0.05$) where groups that do not contain the same letter are different. Exact p -values for (b) are given in Table S1. Regions with mean annual rainfall of 0-300 mm ($n = 362$) and 300-600 mm ($n = 10,333$) had the lowest q values, followed by regions with 600-900 mm ($n = 6,070$), 900-1200 mm ($n = 2,917$), and 1200-1500 mm ($n = 5,091$) of annual rainfall. Median q values were highest in regions with the highest annual rainfall (>1500 mm, $n = 1,395$). For both plots, only events where LAI ≥ 0.5 are included, except for the “bare soil” category, which includes all events where LAI < 0.5 from any IGBP class except for urban and open water cover types.



Extended Data Fig. 2 | Distributions of the median values of the nonlinear parameter, q , by (a) vegetation type and (b) mean annual precipitation. Curves show the kernel density estimates of the distribution of median q values for each class, obtained by resampling from the respective distributions of q . Dashed lines show the median values of the original distributions.



Extended Data Fig. 3 | Observed values of (a) the nonlinear parameter, q , and (b) critical soil moisture threshold, θ^* , by soil sand fraction. Violin plots show the distribution of q values in each category. Box plots show the medians (center line) and 25th to 75th percentile of q values; whiskers extend 1.5 times the inter-quartile range from each box. Outliers beyond this range are denoted by points. The dashed line in (a) shows where $q=1$. Letters denote statistically significant differences between median values (two-sided Dunn's test with Bonferroni correction, $p<0.05$) where groups that do not contain the same letter

are different. Exact p -values for (a) are given in Table S2. All groups in (b) were significantly different from each other at $p<0.0001$. Median q values did not show a coherent trend with sand fraction; locations with 0–20% sand ($n=1,222$) had the highest q values, followed by those with the highest sand fraction (>80%, $n=1,577$). Soils comprised of 40–60% sand ($n=1,338$) had q values very close to 1, while those with 20–40% sand ($n=1,604$) and 60–80% sand ($n=733$) had lower q values. On the other hand, θ^* showed a clear trend, decreasing with increasing sand fraction. For both plots, only events where $LAI \geq 0.5$ are included.

Extended Data Table 1 | Summary statistics and uncertainty estimates for q by vegetation type and rainfall

Category	Class	Median q	95% CI	n
Vegetation type	Grasslands	0.85	[0.83, 0.87]	11,252
	Savannas	1.01	[0.97, 1.05]	5,909
	Woodlands	1.08	[1.05, 1.1]	9,586
Mean annual rainfall	0–300 mm	0.75	[0.69, 0.81]	362
	300–600 mm	0.86	[0.83, 0.87]	10,333
	600–900 mm	1.0	[0.97, 1.04]	6,070
	900–1200 mm	0.99	[0.95, 1.05]	2,917
	1200–1500 mm	1.06	[1.03, 1.09]	5,091
	>1500 mm	1.27	[1.2, 1.4]	1,395

Confidence intervals (CI) were calculated from the bootstrapped distributions shown in Extended Data Fig. 2.

Extended Data Table 2 | Coefficients of the surfaces in Fig. 4

Vegetation type	$c_{AI_{60}}$	c_{LAI}	$c_{AI_{60},LAI}$	c	R^2
Grasslands	0.65	0.02	-0.13	0.55	0.77
Savannas	1.86	0.14	-0.36	-0.037	0.77
Woodlands	0.67	0.10	-0.14	0.62	0.53

See Methods for the full equation.

Reporting Summary

Nature Portfolio wishes to improve the reproducibility of the work that we publish. This form provides structure for consistency and transparency in reporting. For further information on Nature Portfolio policies, see our [Editorial Policies](#) and the [Editorial Policy Checklist](#).

Statistics

For all statistical analyses, confirm that the following items are present in the figure legend, table legend, main text, or Methods section.

n/a Confirmed

- The exact sample size (n) for each experimental group/condition, given as a discrete number and unit of measurement
- A statement on whether measurements were taken from distinct samples or whether the same sample was measured repeatedly
- The statistical test(s) used AND whether they are one- or two-sided
Only common tests should be described solely by name; describe more complex techniques in the Methods section.
- A description of all covariates tested
- A description of any assumptions or corrections, such as tests of normality and adjustment for multiple comparisons
- A full description of the statistical parameters including central tendency (e.g. means) or other basic estimates (e.g. regression coefficient) AND variation (e.g. standard deviation) or associated estimates of uncertainty (e.g. confidence intervals)
- For null hypothesis testing, the test statistic (e.g. F , t , r) with confidence intervals, effect sizes, degrees of freedom and P value noted
Give P values as exact values whenever suitable.
- For Bayesian analysis, information on the choice of priors and Markov chain Monte Carlo settings
- For hierarchical and complex designs, identification of the appropriate level for tests and full reporting of outcomes
- Estimates of effect sizes (e.g. Cohen's d , Pearson's r), indicating how they were calculated

Our web collection on [statistics for biologists](#) contains articles on many of the points above.

Software and code

Policy information about [availability of computer code](#)

Data collection All data processing and analyses were performed in Python 3.12. A custom python package was developed to process the soil moisture drydowns and fit the nonlinear model. This package is available on GitHub at <https://github.com/ecohydro/drydowns>.

Data analysis The code for performing the analyses and creating the figures in this study is available at <https://github.com/ecohydro/ismn-drydowns>.

For manuscripts utilizing custom algorithms or software that are central to the research but not yet described in published literature, software must be made available to editors and reviewers. We strongly encourage code deposition in a community repository (e.g. GitHub). See the Nature Portfolio [guidelines for submitting code & software](#) for further information.

Data

Policy information about [availability of data](#)

All manuscripts must include a [data availability statement](#). This statement should provide the following information, where applicable:

- Accession codes, unique identifiers, or web links for publicly available datasets
- A description of any restrictions on data availability
- For clinical datasets or third party data, please ensure that the statement adheres to our [policy](#)

All soil moisture data used in this study are available from the International Soil Moisture Network (Dorigo et al., 2011; Dorigo et al., 2021; <https://ismn.earth/en/>). The PET data are available from Singer et al. (2021), accessible at <https://data.bris.ac.uk/data/dataset/qb8ujazzda0s2aykkv0oq0ctp>. CHIRPS rainfall data are available from the Climate Hazards Center (<https://www.chc.ucsb.edu/data/chirps>). MODIS Landcover and LAI data were retrieved from NASA's Application for

Research involving human participants, their data, or biological material

Policy information about studies with [human participants or human data](#). See also policy information about [sex, gender \(identity/presentation\), and sexual orientation](#) and [race, ethnicity and racism](#).

Reporting on sex and gender

N/A

Reporting on race, ethnicity, or other socially relevant groupings

N/A

Population characteristics

N/A

Recruitment

N/A

Ethics oversight

N/A

Note that full information on the approval of the study protocol must also be provided in the manuscript.

Field-specific reporting

Please select the one below that is the best fit for your research. If you are not sure, read the appropriate sections before making your selection.

Life sciences

Behavioural & social sciences

Ecological, evolutionary & environmental sciences

For a reference copy of the document with all sections, see nature.com/documents/nr-reporting-summary-flat.pdf

Ecological, evolutionary & environmental sciences study design

All studies must disclose on these points even when the disclosure is negative.

Study description

Briefly describe the study. For quantitative data include treatment factors and interactions, design structure (e.g. factorial, nested, hierarchical), nature and number of experimental units and replicates.

Research sample

The study uses soil moisture data from 1,268 stations in the International Soil Moisture Network (ISMN), the largest global network of in-situ soil moisture data. The sites were divided by vegetation type focusing on three categories: grasslands, savannas, and woodlands/forests. Ancillary data for each site and event analyzed included soil texture, leaf area index, aridity index, and mean annual rainfall.

Sampling strategy

All available soil moisture data from 0-50cm and stations were used. A total of 26,747 soil moisture drydown events were analyzed across all stations.

Data collection

No data were collected in this study. Soil moisture data were obtained from the ISMN, which aggregates daily measurements from sensors worldwide. The study used MODIS data to classify vegetation type and LAI. Climate data, including precipitation and potential evapotranspiration, were obtained from CHIRPS and dPET datasets.

Timing and spatial scale

All available data from the ISMN were used. The availability of the data varies by site. Drydown events were extracted for the entire record and include events from 2001-2022. All data represent point-based soil moisture measurements.

Data exclusions

Events with incomplete data, low goodness-of-fit in model estimations, or spurious parameter values were excluded. Events were also excluded if plant-available water was below a minimum threshold, ensuring that the analyzed dataset represented meaningful vegetation responses to soil drying.

Reproducibility

The study utilized standardized, globally accessible datasets (e.g., ISMN, MODIS, CHIRPS), which supports reproducibility. The methods for data filtering and model fitting were also documented, allowing replication. All code are publicly available to reproduce the results.

Randomization

Randomization was not applicable, as the study relied on observational data collected globally. However, the broad spatial and temporal scope of the sampling ensures that the findings are generalizable.

Blinding

Blinding was not applicable since the study did not involve experimental treatments or subjective observations that could introduce bias.

Did the study involve field work?

Yes

No

Reporting for specific materials, systems and methods

We require information from authors about some types of materials, experimental systems and methods used in many studies. Here, indicate whether each material, system or method listed is relevant to your study. If you are not sure if a list item applies to your research, read the appropriate section before selecting a response.

Materials & experimental systems

n/a	Involved in the study
<input checked="" type="checkbox"/>	Antibodies
<input checked="" type="checkbox"/>	Eukaryotic cell lines
<input checked="" type="checkbox"/>	Palaeontology and archaeology
<input checked="" type="checkbox"/>	Animals and other organisms
<input checked="" type="checkbox"/>	Clinical data
<input checked="" type="checkbox"/>	Dual use research of concern
<input checked="" type="checkbox"/>	Plants

Methods

n/a	Involved in the study
<input checked="" type="checkbox"/>	ChIP-seq
<input checked="" type="checkbox"/>	Flow cytometry
<input checked="" type="checkbox"/>	MRI-based neuroimaging

Plants

Seed stocks

N/A

Novel plant genotypes

N/A

Authentication

N/A